The Cryosphere Discuss., doi:10.5194/tc-2016-259, 2016
Manuscript under review for journal The Cryosphere
Published: 21 November 2016

The Cryosphere Discussions
Open Access
EGU

1

Complex Principal Component Analysis of Mass Balance Change on Qinghai-Tibet Plateau

Jingang Zhan [1], Hongling Shi [1], Yong Wang [1*], Yixin Yao[1,2]

[1]State Key Laboratory of Geodesy and Earth's Dynamics, Institute of Geodesy and Geophysics, Chinese Academy of Sciences, Wuhan 430077, China

[2]University of Chinese Academy of Sciences, Beijing 100049, China

Correspondence to: Yong Wang (ywang@whigg.ac.cn)

Abstract. This paper analyzes the spatial characteristics of mass balance change on the Qinghai-Tibet Plateau and surrounding areas, using 153 monthly solutions of temporal gravity data from the Gravity Recovery and Climate Experiment(in this case GRACE) satellite. Spatial mode characteristics and phase information of mass balance change are analyzed using complex principal component analysis(in this case CPCA). Information on time-frequency change of major components is analyzed using the wavelet amplitude-period spectrum. The results show that the mass balance change on the plateau is influenced by various atmospheric circulations and there are obvious systemic differences, namely, glacial fluctuation of the Himalayas area was mainly influenced by the weakening Indian monsoon, El Niño and East Asian monsoon. There were drastic changes of glacier mass gain and loss balance. Apart from the Indian monsoon and El Niño affected on mass balance in inland areas of the plateau, the northern parts of the plateau was also affected by the westerlies and there was a positive mass balance, with mass gain exceeding loss. The Pamirs and the Karakoram Range areas are influenced not only by the Indian monsoon and westerlies but also by the climate change of El Niño and La Niña, and mass change shows a weak mass balanced. The major influence on the change of mass balance on the Qinghai-Tibet Plateau was the weakening Indian monsoon, which was responsible for 54.0% of that change. Because El Niño is strengthening, it has recently become the second major factor affecting the change of mass balance, responsible for 16.3% of that change. The third major influence was the westerlies and of La Niña-related climate change, accounting for 5.6% of the mass balance change.

1 Introduction

The continuous rise of global sea levels presents a great challenge to the living environment of mankind. For example,

The Cryosphere Discuss., doi:10.5194/tc-2016-259, 2016
Manuscript under review for journal The Cryosphere
Published: 21 November 2016

storm tides strike coastal areas more frequently and flooding damage is increasing. The erosion of coasts and coastal lowlands causes beaches to recede. Water in coastal regions becomes polluted and farmlands are under threats to sanitation. In one hand, seawater absorbs heat and expands, causing global sea levels to rise (Willis, 2003; Antonov et al., 2005). On the other hand, the rise of temperature accelerates the melt speed of polar ice caps and glaciers on land, with part of the meltwater directly (meltwater of polar ice caps) or indirectly (meltwater of glaciers) entering the sea through runoff, also raising sea levels (Nguyen and Herring, 2005, Anny and Frédérique, 2011; Shi et al., 2011; Church et al., 2013). Furthermore, the melting of glaciers accelerates the loss of freshwater resources by which humans live. All these are results of global climate change.

As the cryosphere of the so-called "Third Pole," the Qinghai-Tibet Plateau contains numerous glaciers and lakes water resources. Covering an area of 47,000 km^2, these glaciers are the headstreams of many famous Asian rivers. The plateau is famous for its altitude and vast territory, with a complicated developing environment for glaciers and a changeable climate. For example, the southern and southeast parts of the plateau are under the influence of the Indian monsoon and East Asian monsoon circulations, which bring abundant summer rain. The western part, where the Pamirs are located, is under the influence of westerlies that produce dry and rainless areas. However, the interior of the TBP is less influenced by aforementioned circulations and is dominated more by continental climatic conditions (Yao et al., 2012; Yi and Sun, 2014). The difference between their results is that Yi et al. believed that the Indian monsoon is so much stronger than the westerlies and thus it can also influence Pamirs precipitation in winter and summer. Compared with the findings of Yao et al., Yi and Sun neglected the influence of the East Asian monsoon. However, we hold that the developing environment of glaciers on the Qinghai-Tibet Plateau is more complicated (as shown in Figure 1), because in recent years the El Niño phenomenon has become frequent and is gradually strengthening. Thus, we have enough evidence to believe that this phenomenon will influence the development of glaciers on the plateau.

A glacier is the most sensitive and direct information carrier of climate change. Their melting process records the most direct and detailed dynamic change information of local or even global climate. Glaciologists and meteorologists reproduce ancient climates and the environment by analyzing data of samples taken from glaciers in plateau areas. They then study the response relationships between glaciers and ancient climate change on long time scales and forecast likely future climate change (Thompson et al., 2006; Yao and Yu, 2007; Yao et al., 2012). However, for plateaus with sparse populations, it is obviously unrealistic to obtain glacier time sequences with high spatial

The Cryosphere Discuss., doi:10.5194/tc-2016-259, 2016
Manuscript under review for journal The Cryosphere
Published: 21 November 2016

resolution.

The development of space geodetic technology, especially that of earth observation from space, provides researchers with high precise and continuous earth observation data in terms of glacier mass change and water storage variation in untraveled regions. With these data, unprecedented research achievements have been made in evaluating mass balance in polar and Asian alpine regions (Chen et al., 2009; Matsuo and Heki, 2010; Chen et al., 2011; Gardelle et al., 2012; Jacob et al., 2012; Matsuo and Heki 2012; Yao et al., 2012; Gardelle et al., 2013; Gardner et al., 2013; Yi and Sun, 2014; Xiang et al., 2016). In the application of GRACE, their methods are generally similar. After subtracting signals from the glacial isostatic adjustment (GIA) model, and the terrestrial water storage (TWS) model from the GRACE observation data, the residual gravity change can be totally attributed to changes in glaciers. However, there is a lack of necessary analysis of the dissimilarity of spatial variation and its causes.

The change of mass balance in the cryosphere is the result of interactions between glaciers and atmosphere at different spatial and time scales. To study the time-varying spatial change of mass balance on the Qinghai-Tibet plateau, principal component analysis (PCA) is a useful method (Fenogliomarc, 2000; Wang et al., 2000). The most advantage of PCA is that it can describe complicated changes of initial datasets with fewer variables. However, traditional PCA can detect only standing wave, not advancing waves, because of a lack of corresponding phase information. To overcome this disadvantage, Wallace and Dickinson (2010) developed the complex principal component analysis in the frequency domain (FDPC) method. This performs principal component analysis by calculating vectors of complex features of a relative spectrum matrix. FDPC is the most common method to study spatiotemporal transmission characteristics. However, if climate change fluctuates over irregular time intervals and the energy of its principal component is distributed in multi-frequency bands, the spatial change image of every frequency spectrum must be analyzed. In such a case, it is inconvenient to use FDPC. Compared with FDPC, complex principal component analysis (CPCA) in the time domain is attractive (Horel, 1984). The CPCA method transforms original data and its Hilbert transform into a complex time sequence and conducts principal component analysis by calculating the covariance or complex characteristics vector of the cross-correlation matrix. CPCA is an FDPC method for a full-frequency band. When datasets only have a single frequency, CPCA is equivalent to FDPC. Therefore, CPCA can be used to effectively detect transmitting characteristics, especially when the variance of the principal component is distributed across many frequency bands.

The Cryosphere Discuss., doi:10.5194/tc-2016-259, 2016
Manuscript under review for journal The Cryosphere
Published: 21 November 2016

In this paper, the 153 approximately monthly gravity solutions from the GRACE Release 05 data have been used to reproduce the spatial change of mass balance on the Qinghai-Tibet Plateau. Then, the main components and its corresponding spatial modes and time variation of the mass balance in this area are studied by using the complex principal component analysis technique. The period of each principal component and its time evolution are also studied by using the wavelet amplitude-period Spectrum Analysis in order to explore the possible reasons for the spatial difference of mass balance in the Qinghai Tibet Plateau. It is very helpful for us to understand the respond relationship of mass balance to climate change in this region, and is of great significance to assess the potential impacts of glacier melting on water resources, ecology and environmental disasters.

2 Data

The variation of earth's gravity field reflects the redistribution of mass inside the earth. Over a short time (compared with geologic time), it can be regarded as mass transfer of the earth's surface and shallow fluid. GRACE, which was jointly developed by America and Germany, has been successfully operating for over 10 years. Its monthly gravity solutions have been able to reflect the changes of 1-mm geoid fluctuation in 300-km spatial scale and can be used to monitor gravity field variations caused by the change of hydrology and cryosphere, earthquakes and glacial isostatic adjustment (Ramillien et al., 2006; Chen et al., 2007; Chen et al., 2008; Velicogna, 2009; Rignot et al., 2011).

The time-varying gravity model used in this paper is the Release-05 (RL05) solutions provided by the Center for Space Research (CSR), University of Texas at Austin. The 153 approximately monthly GRACE gravity solutions cover the period January 2003 through September 2015 (~12 solutions are missing), each of which consist of normalized spherical harmonic (SH) coefficients, to degree and order 60. The main improvements in the new products are the mean gravity model and corrections of various new tide models. Some processing algorithms and parameters have also been improved, regarding alignments between the star camera data rate, accelerometer, and K-band system (Bettadpur, 2012). Compared with previous data, the RL05 gravity solutions substantially reduced the stripe noise. However, filtering is still necessary to suppress high-degree and order terms error. In our study, the smoothness priors method (Tarvainen et al., 2002) was used to remove stripe noise in GRACE data.

The Cryosphere Discuss., doi:10.5194/tc-2016-259, 2016
Manuscript under review for journal The Cryosphere
Published: 21 November 2016

5

3 Method

3.1 Equivalent Water Height

According to Wahr et al., [1998], surface mass change can be expressed in the form of surface equal water height (EWH) as

$$\Delta\sigma(\theta,\ \lambda)=\frac{a\rho_e}{3\rho_w}\sum_{n=0}^{\infty}\frac{2n+1}{1+k_n}\sum_{m=0}^{n}\left\{\left[\tilde{c}_n^m\cos(m\lambda)+\tilde{s}_n^m\sin(m\lambda)\right]\tilde{P}_n^m(\cos\theta)\right\} \quad (1)$$

where ρ_e is average density of the earth, a is the equatorial radius, and ρ_w is water density. Parameter λ is colatitude, θ is latitude, and $\tilde{P}_n^m(\cos\theta)$ is the nth-degree and mth-order fully normalized Legendre function. Parameter k_n is the load Love number. $\tilde{c}_n^m$ and $\tilde{s}_n^m$ are the normalized SH coefficients.

3.2 CPCA

For the CPCA, a complex observation sequence should first be constructed, which is different from the PCA. For a time varying observation vector $u_j(t)$, its Fourier expansion is:

$$u_j(\mathrm{t})=\sum_{\omega}\left[a_j(\omega)\cos(\omega t)+b_j(\omega)\sin(\omega t)\right]. \quad (2)$$

In this expansion, j stands for the location of the observation point, t is the observation time, and ω is the Fourier frequency. Its complex form is

$$u_j(t)=\sum_{\omega}c_j(\omega)e^{-i\omega t}. \quad (3)$$

Here, $c_j(\omega)=a_j(\omega)+ib_j(\omega),\mathrm{i}=\sqrt{-1}$. According to the definition of $c_j(\omega)$, Eq. (3) can be expanded as

$$\begin{aligned}U_j(t)&=\sum_{\omega}\left[a_j(\omega)\cos(\omega t)+b_j(\omega)\sin(\omega t)\right]+i\left[b_j(\omega)\cos(\omega t)-a_j(\omega)\sin(\omega t)\right]\\&=u_j(t)+i\mathrm{v}_j(t)\end{aligned}. \quad (4)$$

The real part of Eq. (4) is the original observation sequence and the imaginary part is the Hilbert transform of the real part, which does not change the amplitude of each component of $u_j(t)$. However, the phase of each spectral component is advanced by $\pi/2$.

The traditional PCA is the principal component analysis of the real observation vector, whereas the CPCA analysis is

The Cryosphere Discuss., doi:10.5194/tc-2016-259, 2016
Manuscript under review for journal The Cryosphere
Published: 21 November 2016

the principal component analysis of the complex vector constructed. After the normalization of the complex observation vectors, that is the average value is subtracted from the complex observation vector of each observation point, and then divided by the standard deviation the complex correlation matrix of the observation point can be expressed as:

$$\begin{bmatrix} r_{11} & r_{12} & \cdots & r_{1n} \\ r_{21} & r_{22} & \cdots & r_{2n} \\ \vdots & \cdots & \cdots & \vdots \\ r_{n1} & r_{n2} & \cdots & r_{nn} \end{bmatrix}. \quad (5)$$

Here r_{jk} represents the multiple correlation coefficients between the *j*th and *k*th observation points. CPCA compresses information using the least complex eigenvector e_{jn} of correlation matrix (Eq. 5) and the complex principal component $p_n(t)$, because the correlation matrix (5) is a Hermitian matrix including n real eigenvalues λ. $\lambda_j / \sum_{i=1}^{n} \lambda_i$ denotes the contribution percentage of the *j*th principal component.

Observation vector $U_j(t)$ can be expressed as the sum of N principal components,

$$U_j(t) = \sum_{n=1}^{N} e_{jn}^{*} p_n(t), \quad (6)$$

where * stands for the complex conjugate, and both complex principal components and complex eigenvectors are orthogonal. The *n*th complex eigenvector element e_{jn} can be expressed as

$$e_{jn} = \left[U_j(t) * p_n(t) \right]_t = s_{jn} e^{i\theta_{jn}}. \quad (7)$$

Where, e_{jn} indicates the multiple correlation relationship between the jth time sequence and nth principal component. s_{jn} and θ_{jn} are respectively correlative order of magnitude and phase. $[\cdots]_t$ signifies the average of times. The time sequence elements of principal components can be expressed as the functional form of amplitude T_n and phase Φ_n.

$$P_n(t) = T_n(t) e^{i\Phi_n(t)} \quad (8)$$

The Cryosphere Discuss., doi:10.5194/tc-2016-259, 2016
Manuscript under review for journal The Cryosphere
Published: 21 November 2016

3.3 Wavelet Amplitude-period Spectrum Analysis

Mass balance on the Qinghai-Tibet Plateau is under the influence of climate change, and exhibits unsteady quasi-periodic change. After the temporal change series of principal components in the area are obtained, the time-varying changes of the periods and amplitude (energy) should be analyzed. Here, we use the wavelet amplitude-period spectrum to analyze its time-frequency information, and choosing Morlet wavelet (Morlet et al., 2012) as the basic wavelet. The wavelet amplitude-period spectrum reflects the time-varying amplitude and period of each periodic term (or standardized periodic term). This means that in this spectrum, the location of extreme points corresponds to the instant period of a periodic signal (or quasi periodic term) at that moment, whereas the extreme point value corresponds to the instantaneous amplitude of a certain period signal at that moment. The wavelet amplitude-period spectrum of a time sequence *f(t)* is defined as

$$W_\psi f(a,b) = \frac{1}{aC_\psi}\int_{-\infty}^{\infty} f(t)\psi\left(\frac{t-b}{a}\right)dt, \quad a,b \in R, \quad a \neq 0, \tag{9}$$

where $\psi(t) = e^{\frac{-t^2}{2\delta^2}}\cos(2\pi\omega_0 t), \quad \delta, \omega_0 \in R, 2\pi\delta\omega_0 \gg 1.\ C_\psi = \int_{-\infty}^{\infty}\psi(t)\cos(2\pi\omega_0 t)dt$

Here, the kernel function $\psi(t)$ is the real part of the Morlet wavelet, δ is a constant, and ω_0 is the frequency parameter.

4 Mass change and its CPCA analysis

Figure 2 shows the trend of mass balance on the Qinghai-Tibet Plateau during the period 2003 to 2015. From figure 2, we can see that mass balance on the Qinghai-Tibet Plateau has two major change characteristics, namely, a large negative signal with mass decrease around the southern edge of the Plateau (Himalayas and its southern region) and a positive signal with mass increase in inland areas of the plateau. However, in the Pamirs region, mass variation had no obvious trend. Here, we analyzed mass variation in the area during 2003–2015 using CPCA in order to analysis the reasons for mass change. Table 1 shows the corresponding eigenvalues of the first five principal components and their contribution percentages to mass change in this area. We took the example of the first three principal components for explanation and description. According to table 1, the result from CPCA analysis of the mass variation in Qinghai-Tibet plateau shows that the eigenvalues of the first, second and third principal components are respectively

The Cryosphere Discuss., doi:10.5194/tc-2016-259, 2016
Manuscript under review for journal The Cryosphere
Published: 21 November 2016

82.65, 25.06 and 8.63, and their contribution percentages 54%, 16.37% and 5.64%, which could explain 76.04% of the variation of mass balance in the area.

Figure 3a is the first spatial mode and its spatial phase distribution (arrows) from the CPCA analysis of the mass balance change in the area. According to the figure, the first spatial mode shows change characteristics of three areas: two negative signals of the eastern part of the Himalayas to the Hengduan Mountains (AB area) and the Pamirs to the Karakorum Mountains (D area), and a positive signal of the northwestern part of India (H area). The direction of the arrows indicates the sequence of mass change and the arrow size the change rate of mass. It is obvious from the phase information that the first spatial mode mainly reflects the character of mass change, which is from south to north.

Figure 3b and 3c are the time evolution of the first principal component and its wavelet amplitude-period spectrum analysis results, respectively. It can be seen in the figure 3c that the periodic component that affect the first spatial mode is mainly annual periodic signal, its period and amplitude are relatively stable. According to the result of the time-sequence wavelet amplitude-period spectrum, the period components of the first spatial mode time sequence are very simple, which are single annual-period signals featuring steady periods. The result of its wavelet amplitude-period spectrum is the same as the result of the wavelet amplitude-period spectrum of the Indian monsoon indices time sequence (Figure 3d).

From the phase information of mass variation, it can be inferred that the first spatial mode in the area is strongly controlled by the Indian monsoon, revealing the influence of that monsoon on rainfall in various areas and its spatial evolution. A branch of the monsoon enters the Qinghai-Tibet Plateau via the AB area and proceeds northward over the Tanggula Mountains with gradually declining energy. It is then blocked by the Qilian Mountains and turns westward, forming a circulation. Another branch proceeds northward and enters the Qiangtang Plateau from the middle and western part of the Himalayas, and is obstructed by the Kunlun and Altun mountains. It then progresses westward into the Pamirs. According to Table 1, the influence of the Indian monsoon accounts for 54% of mass balance change on the Qinghai-Tibet Plateau. According to the time sequence of the spatial mode (Figure 3b), the Indian monsoon has been weakening since 2009, and the change of that monsoon is the main reason for mass balance change in the area.

Figure 4a shows the second spatial mode and its phase information. From this, it is seen that this mode is mainly manifested as three mass change zones of southeast–northwest oriented: a positive signal in the southern Karakorum–northwestern India, two negative signals in the AB area–Qiangtang Plateau (E area)–Karakorum, and the

The Cryosphere Discuss., doi:10.5194/tc-2016-259, 2016
Manuscript under review for journal The Cryosphere
Published: 21 November 2016

195 southern Qilian Mountains. Red arrows in the figure show phase information of the second spatial mode, whose direction change is relatively disordered. They mainly enter the inland plateau from the southeast and affect its mass balance change.

Figure 4b and 4c are respectively the time evolution of the second principal component in the area and its wavelet amplitude-period spectrum analysis. From the result of the wavelet amplitude-period spectrum of its time series, we 200 can see that the periodic component of the second principal component is relatively complicated. It mainly contains a semiannual cycle signal, annual cycle signal, 2–4-year and 6.5-year cycle signals. The semiannual, annual and 6.5-year cycle signals have the strongest energy. Energy of the 2–4-year cycle signal is relatively weak, and their energy are all unstable. Comparing with the wavelet amplitude-period spectrum (Figure 4d) of the El Niño evolution in corresponding periods, it was found that both have 6.5-year and annual cycle signals with consistent phase position. 205 According to the spatial phase information and the wavelet amplitude-period spectrum, we conclude that the second spatial mode in the area is mainly affected by the East Asian monsoon and El Niño. Its influence is largely divided into two branches: one of the branches enters into the Qinghai plateau by through the Sichuan basin; another branch enters the Qiangtang plateau by through the eastern part of Himalayas and extends to the northwest of the plateau, until reaches the Karakorum mountain region and then turn to south.

210 Figure 5a portrays the third spatial mode and its spatial phase distribution information (arrows). From the figure, we can see that the third mode is mainly revealed by the features of two regions, a positive signal in the middle-western area (west of 90°E) and a negative signal in the region of Linzhi (A area). Mass change in other regions is in a weak state of balance. The red arrow in the figure shows phase distribution information of the third spatial mode; its direction shows that the mass change has obvious character from west-to-east. This indicates that the factors behind 215 the change of this mode come from the western part.

Figure 5b and 5c show the time change series of the third spatial mode and its wavelet transform spectrum in the area. From results of this wavelet transform spectrum, the cycle components of this mode mainly contain semiannual, annual, 2–4-year and 6.5-year cycle signals. In contrast with from the second main component, energy of the time series of the third spatial mode mainly concentrates in a 2–6.5-year periodic signal; the annual cycle signal is relatively 220 weak. Except for the 6.5-year signal, energy of the cycle signals is not stable. The phase of the 6.5-year cycle signals in the second and third main components are opposite, which indicates that their driving mechanisms are opposite.

The Cryosphere Discuss., doi:10.5194/tc-2016-259, 2016
Manuscript under review for journal The Cryosphere
Published: 21 November 2016

According to the spatial phase information, we conclude that the third spatial mode is mainly affected by the westerlies and La Niña phenomenon, whose influence can be divided into three branches. One branch moves to north beyond the Karakorum Mountains and enters Tarim Basin, and then reaches to the eastern Qinghai Plateau. Another branch moves to east beyond the west Himalayas and enters into the Qiangtang Plateau, then it meets the East Asian monsoon at 90°E area and is obstructed. The third branch goes southward along the Himalayas and influences northern India. The westerlies are weak in the south and strong in the north, so a clear northeast-southwest boundary of force range (blue line in Fig. 5a) is formed in the inland part of the Qinghai-Tibet Plateau.

5 Discussion

5.1 Mass Change of Mass in Inland Qinghai-Tibet Plateau

In the inland part of the Qinghai-Tibet Plateau, there are three obvious mass increase regions, the Qiangtang Plateau (E area), middle and east of the Kunlun Mountains (F area), and Qinghai Plateau (G area). Their respective annual increases were 4.5, 5.5 and 3.5 GT, much smaller than the 30 GT of Yi et al. (2014). Many scholars have conducted related research in an attempt to explain the reason behind mass balance change in the region.

Mass balance of the Inner Tibet Plateau (ITP) derived from GRACE data showed a positive rate that was attributable to glacier mass gain, whereas those glaciers from other field-based studies showed an overall mass loss. For example, Jacob (2012) deduced the glacier mass balance using GRACE data, finding a mass increase rate of 7 Gt yr^{-1} in the E and F areas. However, according to onsite observation of more than 20 glaciers in Qinghai-Tibet Plateau area (Yao et al., 2012), glaciers in Qinghai-Tibet Plateau area are shrinking dramatically. Their results indicate that the Himalayas shows the most extreme glacial shrinkage based on the reduction both of glacier length and area. The shrinkage is most pronounced in the southeastern TBP, where the length decreased at a rate of 48.2m/yr and the area was reduced at a rate of 0.57% /yr during the 1970s-2000s. The rate of glacial shrinkage decreases from the southeastern TBP to the interior.

Zhang et al. (2013) studied 53% of the total lake area on the plateau using ICESAT satellite data, finding a mass increase rate of 4.95 Gt yr^{-1}. They suggested that the increased mass measured by GRACE was largely due to increased water mass in lakes. If this rate holds true for all lakes, the total mass variance rate is +8.06 Gt yr^{-1} according to the area ratio. However, glacier melting into lakes, itself, should not increase the overall mass and may decrease the

The Cryosphere Discuss., doi:10.5194/tc-2016-259, 2016
Manuscript under review for journal The Cryosphere
Published: 21 November 2016

mass because a portion of the melted water would be lost through evaporation or discharged to rivers that leave the Tibet Plateau.

Yi et al. (2014) indicated a relatively large mass rate change in this area, and explained this change through glacier change, lake water levels, geologic structural processes, and frozen soil. They stated that according to model calculation, the change of inland water storage was −3.3 Gt yr^{-1}. The change of negative balance of weakening glacier mass has been confirmed (Bolch et al., 2010, Bolch et al., 2012, Yao et al., 2012). According to the calculation and estimation of Zhang et al. (2013), the increase of lake water is 8.1 Gt yr^{-1}, and the effect of tectonic movement (simple Bouguer correction) is 0–13 Gt yr^{-1}. The effect of other factors is close to zero. However, we believe that geologic structural processes are slow. Further, we still lack enough observation data of mass balance states in the interior part of the earth in the study region. Thus, the exact Bouguer equilibrium correction requires more scientific data for confirmation.

The effect of soil freezing on mass change in the inland plateau is weak, because the terrain there is flatter than at the plateau edge. The inland area contains numerous lakes and wetlands, which is conducive to the convergence of fluid. Moreover, when water melts and is lost from frozen soil, soil porosity definitely increases, which captures more water during rainy periods.

Based on the results of our work, we tend to believe that rainfall is the main reason for the mass increase in the study region. Data indicate strong evidence that precipitation on the ITP over the past several decades has greatly increased (Yao et al., 2012; Global Precipitation Climatology Project or GPCP, www.esrl.noaa.gov/psd/data/gridded/data.gpcp.html). Influenced by El Niño, moist air moves westward to the inland plateau through the eastern Himalayas and Qinghai, which brings rainfall to the inland and causes rainfall accumulation in plateau lakes and wetland areas. Moreover, the increase of temperature (Qin et al., 2009) accelerates glacial melting in this area. This glacier melting water enters lakes through runoff. It also explains why onsite observation data of glaciers indicate slight shrinkage, and GRACE observations indicate the reason for mass increase.

5.2 Mass Changes of Glaciers in Himalayas Region

The mass reduction rate of glaciers in the entire Himalaya mountain region is 14 Gt yr^{-1}. The mass loss of glaciers in the eastern Himalayas is the most dramatic, with reductions 4.6 Gt yr^{-1} in A area) and 4.1 Gt yr^{-1} in B area). This change trend is consistent with the research of Yao et al. (2012).

The Cryosphere Discuss., doi:10.5194/tc-2016-259, 2016
Manuscript under review for journal The Cryosphere
Published: 21 November 2016

The results of CPCA analysis indicate that the Himalayas and its southern portion are mainly affected by the Indian monsoon climate, and the intensity of this monsoon is weakening. This is consistent with the conclusions of Wu (2005). A weakening Indian monsoon brings less humid air to the study region, causing interannual rainfall decreases. The GPCP rainfall data confirm this. The eastern Himalayas are also affected by El Niño. Glaciers in this area are of a marine type, which mass has large inputs and outputs and is strongly affected by changes of marine climate.

We estimate that the mass loss in northwestern India (H area) is −13.6 Gt yr^{-1}. Rodell et al. (2009) and Yi (2014) gave relatively large values of −17.7 Gt yr^{-1} and −20.2 Gt yr^{-1}, respectively. The reason for this discrepancy might be that Rodell et al. (2009) used data from the RL04 version. Yi et al. (2014) stated that the RL04 solutions tend to overestimate the glacier melting rate of Himalayas by as much as 17%. The difference between our results and those of Yi et al. may be attributable to the difference of solution methods. Moreover, the filtering method may somewhat attenuate the signal.

5.3 Effect of Circulation in Qinghai-Tibet Plateau area

Through observation of some glaciers on the Qinghai-Tibet Plateau area, Yao et al. (2012) discovered that glacier recession in the Himalayas was the most dramatic, followed by the inland plateau. Glaciers in the Pamirs had weak balance changes, and some of the glaciers in the eastern Pamirs Plateau are still expanding. Yao et al. believed that the main reason for this was climates with different circulations. This includes effects of the weakened Indian monsoon in the Himalayas and rainfall decreases. However, there are also effects of the strengthening of the westerlies in the Pamirs and its eastern portion, plus rainfall increases. In the inland plateau, the influences of these two circulations are limited.

Through harmonic analysis of the time series of mass changes in the study region, Yi et al. (2014) found a 5 year periodic signal in the Pamirs and Karakorum regions. Then, they analyzed the correlation of mass change, precipitation, El Niño–Southern Oscillation (ENSO) and Arctic Oscillation (AO), and found that the 5 year undulating signal of mass change is controlled by both the ENSO and the AO.

Yao et al. (2012) considered the effect of the Indian monsoon and westerlies but ignored the phenomenon of El Niño, which is the second major component (16.3%) of the study region. Yi et al. (2014) also noted that the five-year periodic signal in the Pamirs region might be related to ENSO, but ignored the effect of La Niña because they did not distinguish the phase information. According to the CPCA, we believe that the mass change in Qinghai-Tibet Plateau

The Cryosphere Discuss., doi:10.5194/tc-2016-259, 2016
Manuscript under review for journal The Cryosphere
Published: 21 November 2016

area is mainly controlled by the Indian monsoon and westerlies, and the influence of El Niño and La Niña phenomenon in the inland of plateau and Karakorum area cannot be ignored.

6 Conclusion

Mass change on the Tibetan Plateau and surroundings varies systematically from region to region. Specifically, the Himalayas region had the greatest negative mass balance and the continental interior of the plateau had a positive signal with mass increase, whereas the Pamirs had a weak negative mass balance. The main cause of the systematic mass change was the variation of rainfall, which mainly results from changes in four different atmospheric circulation patterns over the Qinghai-Tibet Plateau and surroundings, i.e., the weakening Indian monsoon, strengthened westerlies, El Niño, and La Niña. Their contributions can explain approximately 74% of mass change on the Qinghai-Tibet Plateau.

The Cryosphere Discuss., doi:10.5194/tc-2016-259, 2016
Manuscript under review for journal The Cryosphere
Published: 21 November 2016

Reference:

315 Anny, C. and R. Frédérique : Sea level and climate: measurements and causes of changes, Wiley Interdisciplinary Reviews Climate Change, 2(5): 647-662,2011.

Antonov, J. I., S. Levitus and T. P. Boyer: Thermosteric sea level rise, 1955–2003, Geophysical Research Letters, 32(12): 161-179,2005

Bettadpur, S.: Insights into the Earth System mass variability from CSR-RL05 GRACE gravity fields, EGU General 320 Assembly Conference,2012.

Bolch, T., A. Kulkarni, A. Kääb, C. Huggel, F. Paul, J. G. Cogley, H. Frey, J. S. Kargel, K. Fujita and M. Scheel: The state and fate of Himalayan glaciers, Science 336(6079): 310-314, 2012.

Bolch, T., T. Yao, S. Kang and M. F. Buchroithner: A glacier inventory for the western Nyainqentanglha Range and the Nam Co Basin, Tibet, and glacier changes 1976–2009, Cryosphere Discussions, 4(3): 419-433, 2010.

325 Chen, J. L., C. R. Wilson, D. Blankenship and B. D. Tapley: Accelerated Antarctic ice loss from satellite gravity measurements, Nature Geoscience, 2(12): 859-862, 2009.

Chen, J. L., C. R. Wilson and B. D. Tapley: Interannual variability of Greenland ice losses from satellite gravimetry, Journal of Geophysical Research Atmospheres, 116(B7): 785-814, 2011.

Chen, J. L., C. R. Wilson, B. D. Tapley, D. Blankenship and D. Young: Antarctic regional ice loss rates from GRACE, 330 Earth & Planetary Science Letters, 266(1–2): 140-148, 2008.

Chen, J. L., C. R. Wilson, B. D. Tapley and S. Grand: GRACE detects coseismic and postseismic deformation from the Sumatra-Andaman earthquake, Geophys Res Lett 34(13):L13302, Geophysical Research Letters 34(13): 173-180, 2007.

Church, J. A., N. J. White, L. F. Konikow, C. M. Domingues, J. G. Cogley, E. Rignot, J. M. Gregory, M. R. van den 335 Broeke, A. J. Monaghan, and I. Velicogna: Revisiting the Earth's sea-level and energy budgets from 1961 to 2008 (vol. 38, L18601, 2011), Geophys. Res. Lett., 40, 4066, doi:10.1002/grl.50752, 2013.

Fenogliomarc, L., Y. Wang and E. Groten: Investigation at regional scales of sea level variability at low and medium frequencies, AVISO Newletter N.7, pp.40-43 CNES, 2000.

Gardelle, J., E. Berthier and Y. Arnaud: Slight mass gain of Karakoram glaciers in the early twenty-first century,

The Cryosphere Discuss., doi:10.5194/tc-2016-259, 2016
Manuscript under review for journal The Cryosphere
Published: 21 November 2016

Nature Geoscience, 5(5): 322-325, 2012.

Gardelle, J., E. Berthier, Y. Arnaud and A. Kääb: Region-wide glacier mass balances over the Pamir-Karakoram-Himalaya during 1999-2011, Cryosphere, 7(2): 1263-1286, 2013.

Gardner, A. S., G. Moholdt, J. G. Cogley, B. Wouters, A. A. Arendt, J. Wahr, E. Berthier, R. Hock, W. T. Pfeffer and G. Kaser: A Reconciled Estimate of Glacier Contributions to Sea Level Rise: 2003 to 2009, Science, 340(6134): 852-857, 2013.

Horel, J. D.： Complex Principal Component Analysis: Theory and Examples，Journal of Climatology & Applied Meteorology, 23(12): 1660-1673, 1984.

Jacob, T., J. Wahr, W. T. Pfeffer and S. Swnson: Recent contributions of glaciers and ice caps to sea level rise, Nature, 482(7386): 514-518, 2012.

LG, T., M.-T. E, B. H, D. M, L. B, L. D, L. PN, M. T and M. K: Abrupt tropical climate change: past and present, Proceedings of the National Academy of Sciences of the United States of America, 103(28): 10536-10543, 2006.

Matsuo, K. and K. Heki: Time-variable ice loss in Asian high mountains from satellite gravimetry, Earth & Planetary Science Letters, 290(1–2): 30-36, 2010.

Matsuo, K. and K. Heki: Anomalous precipitation signatures of the Arctic Oscillation in the time-variable gravity field by GRACE, Geophysical Journal International, 190(3): 1495-1506, 2012.

Morlet, J., G. Arens, E. Fourgeau and D. Giard: Wave propagation and sampling theory—Part I: Complex signal and scattering in multilayered media, Geophysics, 47(2): 203, 2012.

Nguyen, A. T. and T. A. Herring: Analysis of ICESat data using Kalman filter and kriging to study height changes in East Antarctica, Geophysical Research Letters, 32(23): 312-329, 2005.

Qin, J., K. Yang, S. Liang and X. Guo: The altitudinal dependence of recent rapid warming over the Tibetan Plateau, Climatic Change, 97(1): 321-327, 2009.

Ramillien, G., A. Lombard, A. Cazenave, E. R. Ivins, M. Llubes, F. Remy and R. Biancale: Interannual variations of the mass balance of the Antarctica and Greenland ice sheets from GRACE, Global & Planetary Change, 53(3): 198-208, 2006.

Rignot, E., I. Velicogna, d. B. Van, M. R., A. Monaghan and J. T. M. Lenaerts: Acceleration of the contribution of the Greenland and Antarctic ice sheets to sea level rise, Geophysical Research Letters, 38(5): 132-140, 2011.

The Cryosphere Discuss., doi:10.5194/tc-2016-259, 2016
Manuscript under review for journal The Cryosphere
Published: 21 November 2016

Shi, H., Y. Lu, Z. Du, L. Jia, Z. Zhang and C. Zhou: Mass change detection in Antarctic ice sheet using ICESat block analysis techniques from 2003 to 2008, Chinese Journal of Geophysics- Chinese Edition, 54(4): 958-965, 2011.

Tarvainen, M. P., P. O. Rantaaho and P. A. Karjalainen: An advanced detrending method with application to HRV analysis, IEEE Transactions on Biomedical Engineering, 49(2): 172-175, 2002.

Velicogna, I.: Increasing rates of ice mass loss from the Greenland and Antarctic ice sheets revealed by GRACE. Geophys Res Lett 36(L19503), Geophysical Research Letters, 36(19): 158-168, 2009.

Wallace, J. M. and R. E. Dickinson: Empirical Orthogonal Representation of Time Series in the Frequency Domain. Part I: Theoretical Considerations, Journal of Applied Meteorology, 11(11): 887-892, 2010.

Willis, A.: The Role of the Global Reporting Initiative's Sustainability Reporting Guidelines in the Social Screening of Investments, Journal of Business Ethics, 43(3): 233-237, 2003.

Wu, B.: Weakening of Indian Summer Monsoon in Recent Decades, Advances in Atmospheric Sciences, 22(1): 21-29, 2005.

Xiang, L., H. Wang, H. Steffen, P. Wu, L. Jia, L. Jiang and Q. Shen: Groundwater storage changes in the Tibetan Plateau and adjacent areas revealed from GRACE satellite gravity data, Earth & Planetary Science Letters, 452:309-320, 2016.

Yao, T., L. Thompson, W. Yang, W. Yu, Y. Gao, X. Guo, X. Yang, K. Duan, H. Zhao and B. Xu: Different glacier status with atmospheric circulations in Tibetan Plateau and surroundings, Nature Climate Change, 2(9): 663-667, 2012.

Yao, T. and W. Yu: Recent Glacial Retreat and Its Impact on Hydrological Processes on the Tibetan Plateau, China, and Surrounding Regions, Arctic Antarctic & Alpine Research, 39(4): 642-650, 2007.

Yi, S. and W. Sun: Evaluation of glacier changes in high-mountain Asia based on 10 year GRACE RL05 models, Journal of Geophysical Research Solid Earth, 119(3): 2504–2517, 2014.

Zhang, G., T. Yao, H. Xie, S. Kang and Y. Lei: Increased mass over the Tibetan Plateau: From lakes or glaciers?, Geophysical Research Letters, 40(10): 2125-2130, 2013.

The Cryosphere Discuss., doi:10.5194/tc-2016-259, 2016
Manuscript under review for journal The Cryosphere
Published: 21 November 2016

17

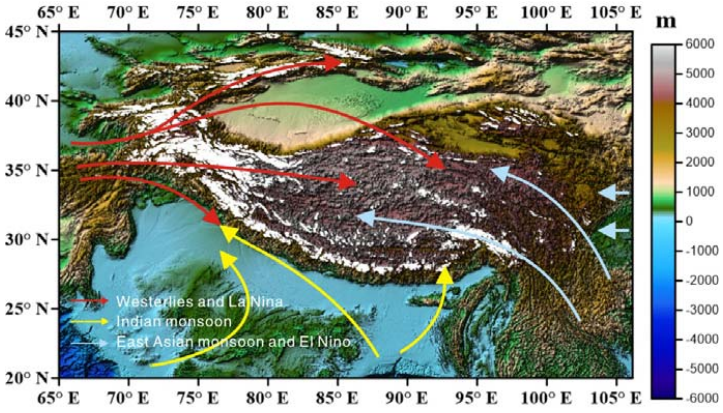

Figure 1: Distribution of glaciers (white dots) and circulation of atmosphere in and round Tibetan Plateau.

395

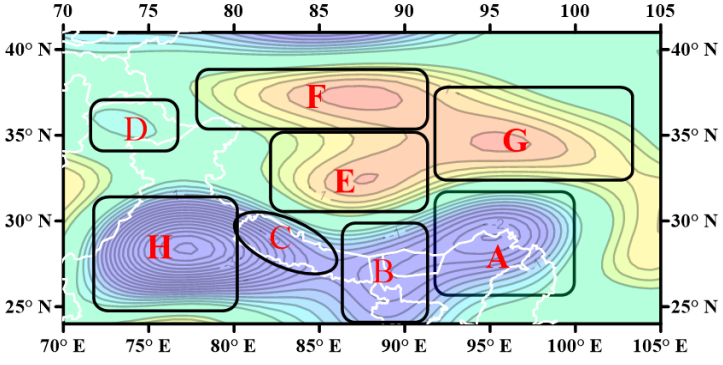

Figure 2 Trend of mass balance in and around Tibetan Plateau

400

405

The Cryosphere Discuss., doi:10.5194/tc-2016-259, 2016
Manuscript under review for journal The Cryosphere
Published: 21 November 2016

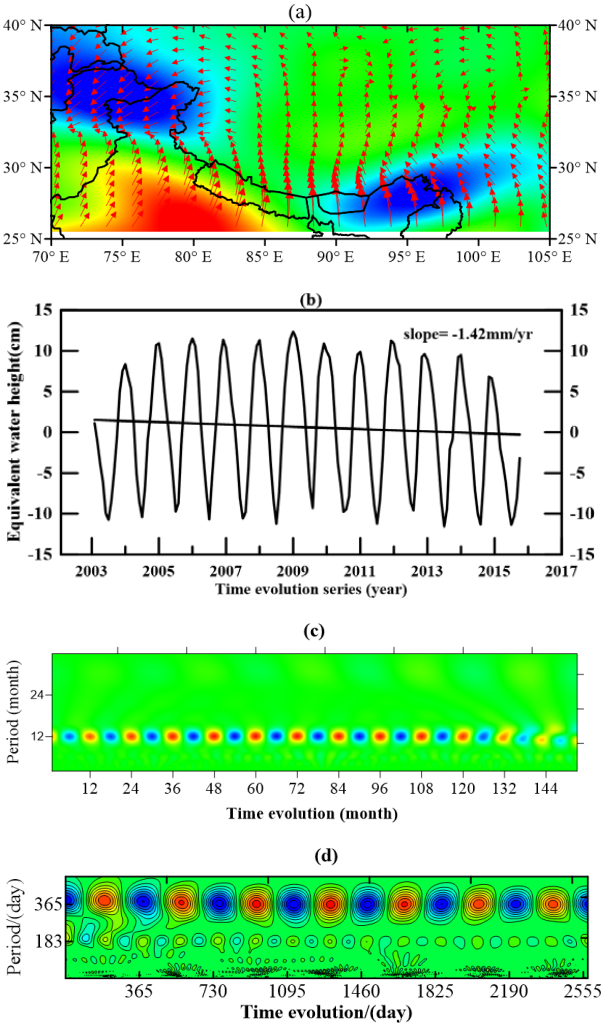

410 **Figure 3: First spatial mode and phase (a), temporal patterns of first principal component (b), and its wavelet amplitude-period spectrum (c) of mass balance change, as well as wavelet amplitude-period spectrum of Indian monsoon indices in period 2003–2009 (d)**

415

The Cryosphere Discuss., doi:10.5194/tc-2016-259, 2016
Manuscript under review for journal The Cryosphere
Published: 21 November 2016

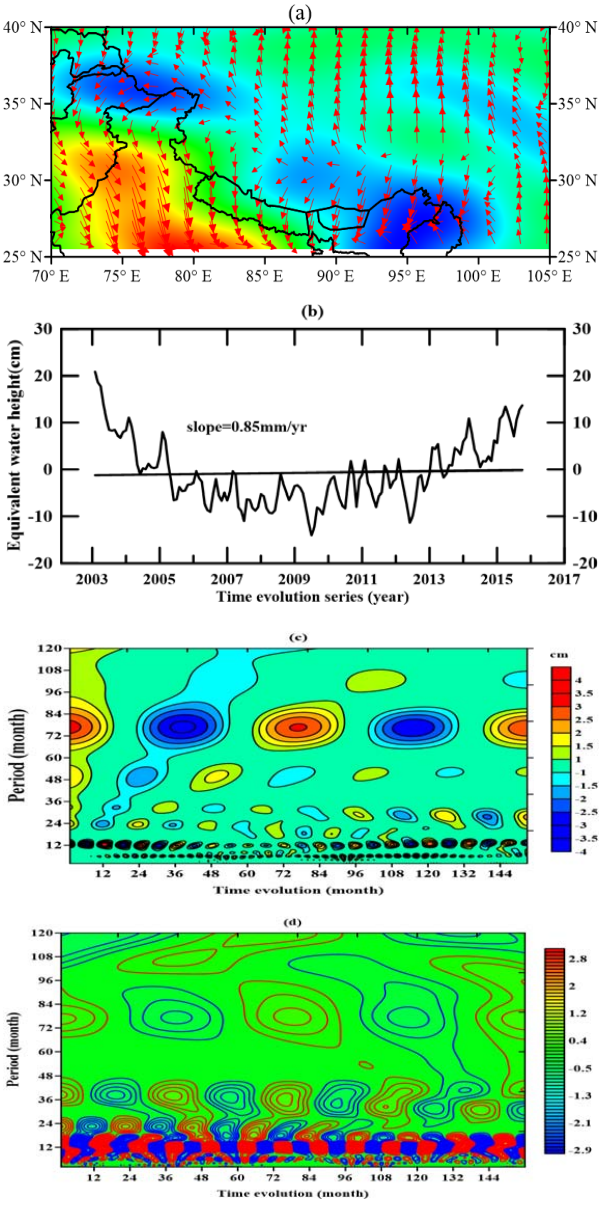

Figure 4: Second spatial mode and phase (a), temporal patterns of second principal component (b), and its wavelet amplitude-period spectrum (c) of mass balance change, as well as wavelet amplitude-period spectrum of El Niño in period 2003–2015 (d)

The Cryosphere Discuss., doi:10.5194/tc-2016-259, 2016
Manuscript under review for journal The Cryosphere
Published: 21 November 2016

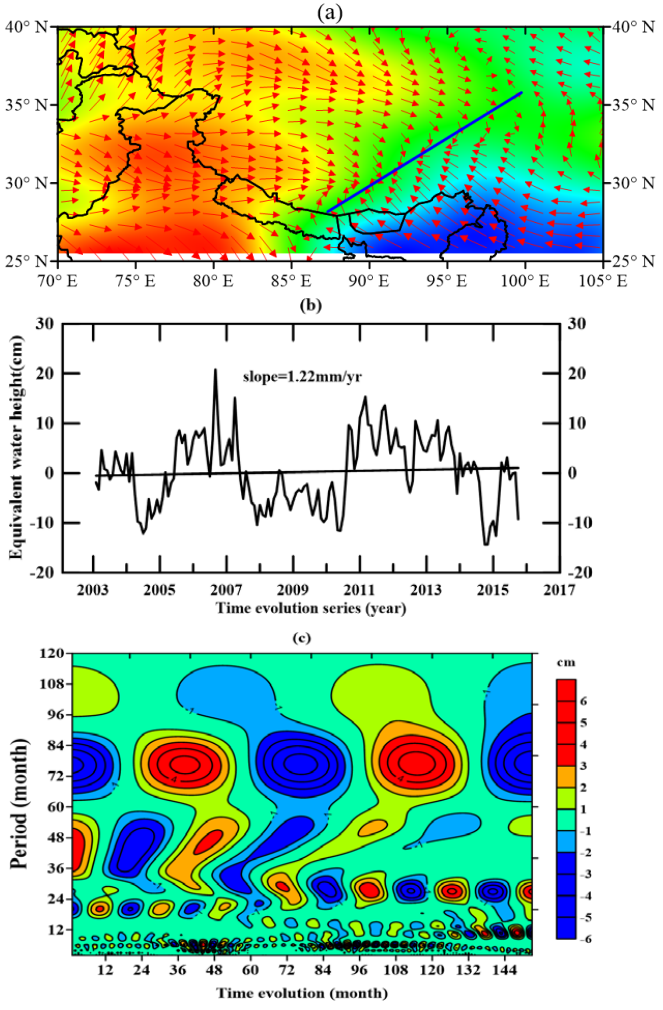

Figure 5: Third spatial mode and phase (a), temporal patterns of third principal component (b), and its wavelet amplitude-period spectrum (c) of mass balance change.

The Cryosphere Discuss., doi:10.5194/tc-2016-259, 2016
Manuscript under review for journal The Cryosphere
Published: 21 November 2016

435 **Table 1 Eigenvalues and contribution percentages to mass change in CPCA analysis of Qinghai-Tibet Plateau**

Number	Eigenvalues	As percentages	Cumul. percentages
1	82.6516	54.02	54.02
2	25.0562	16.38	70.40
3	8.6290	5.64	76.04
4	7.3688	4.82	80.85
5	5.1715	3.38	84.23